Observations from hydrodynamic testing of a flexible, large-diameter monopile in irregular waves

Observations from hydrodynamic testing of a flexible, large-diameter monopile in irregular waves

E E Bachynski[1], M Thys[2], and F H Dadmarzi[1]

[1]Department of Marine Technology, Norwegian University of Science and Technology, Trondheim, Norway
[2] Department of Ships and Ocean Structures, SINTEF Ocean, Trondheim, Norway

E-mail: erin.bachynski@ntnu.no

Abstract.
As the offshore wind industry moves toward larger wind turbines and deeper water, wave-induced loads on large-diameter monopiles are of increasing importance for ultimate limit state design checks. The combination of a relatively large diameter with steep waves in intermediate water depth presents challenges for numerical methods, and small-scale hydrodynamic testing of monopiles is therefore a necessary step in reducing the uncertainties in numerical analyses. Here, we aim to summarize the experimental observations in a new set of tests carried out with a flexible monopile wind turbine, and to understand the similarities and differences between these results and previous studies. Compared to previous studies, the present tests consider a larger monopile diameter and hub height, and include a larger number of realizations and repetitions. The distribution of extreme values and the contributions from different structural modes are studied. These experimental results provide insight into the physical effects which must be accurately captured by numerical tools that are used in design.

1. Introduction

As the offshore wind industry moves toward larger wind turbines in deeper water, wave-induced responses of large-diameter monopiles are of increasing importance for ultimate limit state design checks. In particular, there are concerns about ringing-type responses ("transient structural deflections at frequencies substantially higher than the incident wave frequencies" [1]) due to steep waves, and responses in higher modes due to slamming loads [2].

Compared to existing literature and methods regarding e.g. ringing responses of tension leg platforms, the hydrodynamic problem in intermediate water depth ($\frac{\lambda}{20} < h < \frac{\lambda}{2}$, where h is the water depth and λ is the wave length) requires consideration of the nonlinear incoming wave potential [3] in addition to the nonlinear diffraction effects from the cylinder. Furthermore, the load distribution (not just the total load) is typically more important for a monopile wind turbine than a platform in deep water.

While some advances have been made toward better numerical models, there is still a need for high-quality validation data to better understand the nonlinear wave loads in irregular wave conditions. This problem can be studied experimentally using a rigid monopile model, where the hydrodynamic loads on the model are measured directly [3–5], a model that pitches (giving an approximation of the first mode responses [5, 6], or a model that represents the elasticity of the structure at model scale [2, 7–11]. When using a rigid model, the natural frequencies of the model, including the effects of the measurement equipment, must be sufficiently high such that measurements at the load frequencies of interest are not significantly affected by dynamic responses. A pitching model enables a better understanding of the

first mode response, but does not provide any information about responses in higher modes, and may misrepresent the radiation loads [5]. In the present work, we examine the results of an experimental campaign with a flexible model. The present tests, which are part of the WAS-XL project (Phase II), can be compared to similar tests carried out in several major research projects: WiFi [2, 7, 8], WaveLoads [9, 10], and NOWITECH [11].

Table 1 summarizes the main characteristics of the previous and present experimental campaigns. Full-scale values for the water depth at the model h, diameter D, first and second natural frequencies f_1 and f_2, and estimated total damping level for the first two modes ξ_1 and ξ_2 are shown. During storms with steep waves that excite dynamic responses, the turbine may be shut down due to wind speeds beyond the cut-out speed, resulting in a very lightly damped system. Several important differences between the present tests and previous work can be noted: the monopile diameter is significantly larger than in previous tests, and the second mode damping is relatively low. Except for the WaveLoads tests (which included a ramp), all of these experimental campaigns are carried out with a flat bottom. No estimate of the second mode damping was attempted for the NOWITECH tests.

Table 1: Experimental studies of irregular wave effects on flexible monopiles. *Indicates that the measured damping was nonlinear, only the linear component of the damping is presented.

	scale	h (m)	D (m)	f_1 (Hz)	f_2 (Hz)	ξ_1 (%)	ξ_2 (%)
WiFi [2, 7, 8]	1:30	30	5.8-7.0	0.29	1.21	1.1	1.1
WaveLoads [9, 10, 12]	1:80	20.8-40.8	6.0	0.28	2.0	1.7	1.7
NOWITECH [11]	1:40	30	7.0	0.22	0.85	0.5*	-
WAS-XL Phase II	**1:50**	**27**	**9.0**	**0.25**	**1.58**	**1.1/1.7**	**0.4**

Although the WAS-XL phase II tests included both regular and irregular waves, the focus of the present work is on the irregular wave results. Fig. 1a compares the wave conditions (significant wave height H_s and peak period T_p) from the present tests and previous tests, as well as the 50-year wave contours for different wind speeds at a reference location in the North Sea (Site 15 following Li et al. [13]). The moderate wave conditions in the WaveLoads project as well as the extreme conditions in the WiFi project are similar to the largest sea states in the present tests (see also Table 3). The monopile model, which is illustrated in Fig. 1b and 1c, is discussed in greater detail in Section 2.

Several important observations from previous experimental campaigns are summarized in Table 2. These observations provide some insight into the physical effects which must be captured by numerical tools in order to accurately estimate extreme responses. In the present work, we aim to compare the results from the present tests with these general observations, and to show new contributions of the present tests in terms of repeatability, stochastic variations, and the effects of damping.

Table 2: Selected observations from previous experimental campaigns.

WiFi [2, 7, 8]	- Response at first eigenfrequency roughly 40 % of the max. bending moment - Response at second eigenfrequency 5-20 % of the max. bending moment - Significant response at second eigenfrequency associated with breaking waves
WaveLoads [9, 10]	- Largest accelerations occur for waves close to or within the breaking limits - Strong correlation between inline force and time derivative of wave elevation (η_t)
NOWITECH [11]	- Difficult to assess results due to very low damping - Statistics of max. response are repeatable within 2 % (for individual events, 18 %)

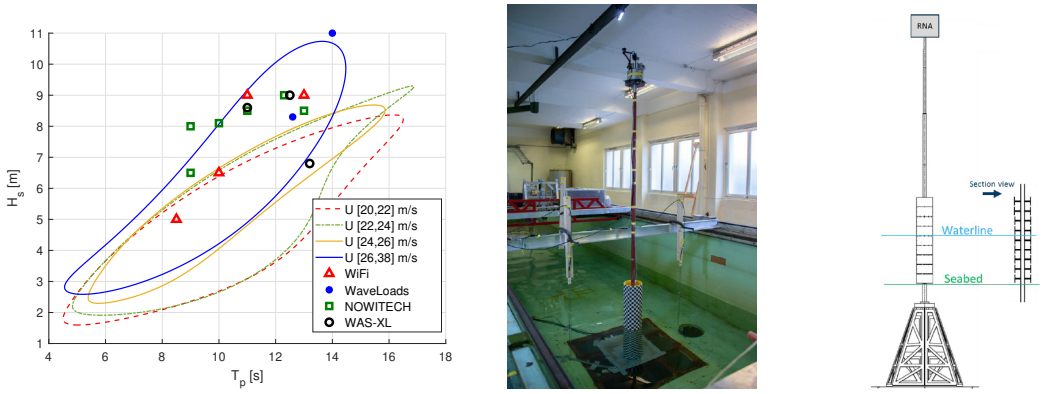

(a) **(b)** **(c)**

Figure 1: a) Environmental conditions in model tests of flexible monopiles in irregular waves, compared to 50-year wave contours for different wind speeds at a reference location in the North Sea (Site 15 [13]). b) Photo of the installed model. c) Sketch showing the model construction.

2. Experimental Setup

2.1. Monopile model and instrumentation

The tower and the monopile (from seabed to top of tower) of a representative 10 MW monopile wind turbine (originally designed for 30 m water depth [14]) are modelled experimentally using an elastic backbone model (Fig. 1b and 1c). The scale of the model is 1:50, and all values are presented at full scale unless otherwise noted. An inner core modelled the desired stiffness while outer shells modelled the correct hydrodynamic diameter. The backbone of the model was made from tubing with varying diameter, and extended below seabed to model the soil stiffness. The outer shell was made out of 5.3 m long segments that were connected to the backbone at the middle of the shell with 0.1 m vertical gaps between the shells, see section view in Fig. 1c. The space between the inner backbone and the outer shells was filled with divinycell (hard plastic foam material) to minimise filling of the space with water.

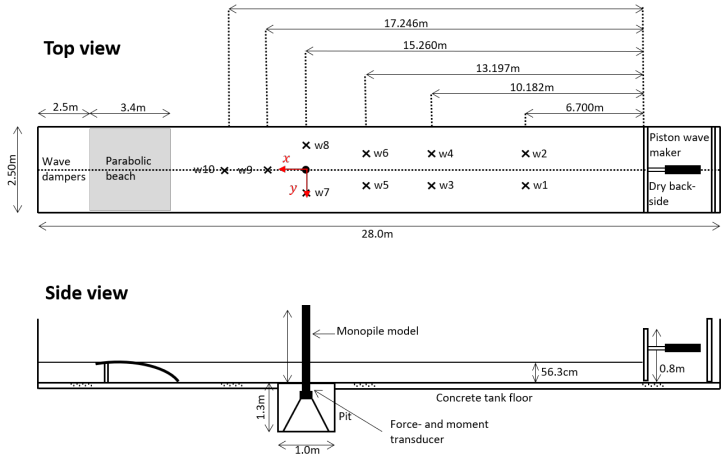

Figure 2: Top and side view of the experimental setup at NTNU/SINTEF Ocean. Dimensions are given in model scale. Wave gauges are indicated by "w."

A mass was mounted on the top of the model to represent the mass of the rotor-nacelle-assembly (RNA). Excluding the RNA and soil spring, the model has a mass of 2652 tonnes and centre of gravity (COG) 36.52 m above seabed. The mass of the RNA was artificially increased from 6.77e5kg to 9.55e5kg

to achieve a first fore-aft eigenfrequency close to 4 s. The elevation of the COG of the RNA is 145.4m above seabed. The moment of inertia due to the rotor was not modelled in the experiments. The combined soil, aerodynamic, and structural damping is modelled by use of a tuned mass damper that was installed at the tower top, and two different damping levels were tested in one of the sea states. The monopile model was not designed to correctly represent higher modes (beyond the second mode). The responses presented herein are therefore low-pass filtered to remove higher frequency components.

Fig. 3 shows the results of decay tests of the model in water. Several sets of tests were carried out to document the first two modes of vibration. As shown, the obtained total damping (including effects of the damper and hydrodynamic damping) in both modes can be approximated as linear. The two damping levels (see Table 1) for the first mode both fall within the range of measured full scale damping (1.05%-2.8% depending on the wind speed and inclusion of tuned mass damper) [15–19]. Fig. 3 shows that the second mode is very lightly damped, and changes in the damper have little effect on the damping of the second mode, which remains close to 0.4 % in all decay tests.

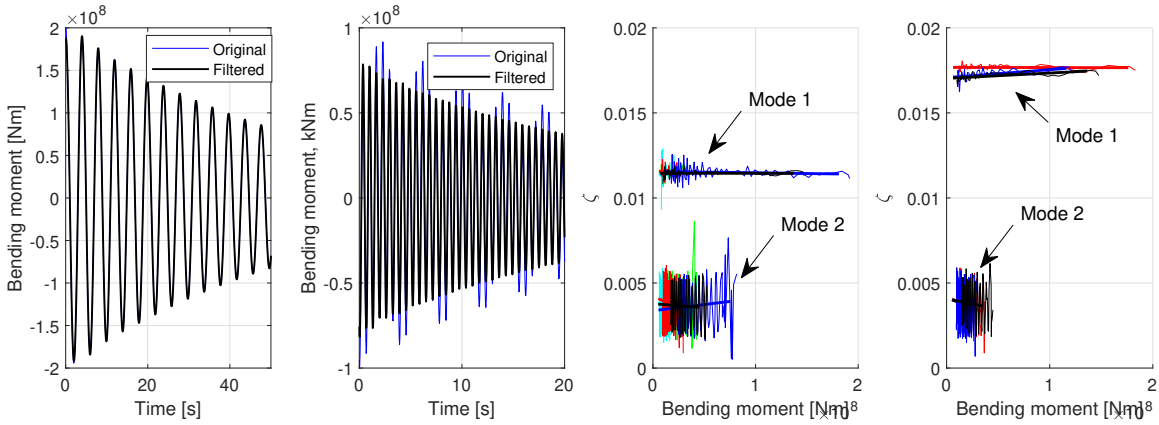

Figure 3: Decay test results. Left (second from left) time series of the bending moment near the mudline after initial force applied at the top (middle), filter is applied around the first (second) natural frequency. Third from left (fourth from left): estimated damping as a function of bending moment near the mudline for several decay tests, baseline model (model with increased damping). Different colors in the right two figures show different decay test realizations.

2.2. Wave conditions

The flexible monopile model was subjected to a range of regular and irregular wave conditions, as summarized in Table 3. In addition to H_s and T_p, we describe the irregular waves by the peakedness parameter (γ) for the JONSWAP spectrum and a measure of the steepness, $s = H_s/\lambda$, where λ is the wavelength associated with the peak period, and is calculated using both the linear and nonlinear dispersion relations (resulting in two values for each sea state).

In the present analysis, we focus solely on the irregular waves that were generated without applying the second order wavemaker correction [20]. The first two sea states were chosen based on the metocean data applied in the WAS-XL project, while the third corresponds to a condition that had previously been tested for the Dudgeon Wind Farm [21]. Tests with increased damping (1.7 % compared to 1.1 % in the majority of the tests) were carried out for one sea state. Each realization consists of 3 hours of full scale data; however, all statistics and results are presented for 2 hours and 42 minutes in order to account for transients in the basin. Wave calibration tests without the model were carried out for all realizations; unless otherwise indicated, the wave elevation that is presented is measured at the origin during the calibration test.

Table 3: Regular and irregular wave conditions tested with the flexible monopile model. "Repetitions" refers to the number of extra runs of one 3-hour wave realization (one seed).

Regular waves						
6.5-16 s, steepness 1/20, 1/22, 1/25, 1/30 and 1/40						all damping levels
Irregular waves without second order correction						
H_s (m)	T_p (s)	γ	s	seeds	repetitions	models
8.6	11.0	4.2	0.057-0.059	20	14	baseline
9.0	12.5	2.6	0.050-0.052	10	5	baseline
6.8	13.2	1.0	0.035-0.037	10	10	baseline
6.8	13.2	1.0	0.035-0.037	10	-	increased damping
Irregular waves with second order correction						
H_s (m)	T_p (s)	γ	s	seeds	repetitions	models
6.8	13.2	1.0	0.035-0.037	10	10+10	baseline

3. Results

3.1. Wave elevation

Fig. 4 shows the exceedance probability distribution for the crest-to-trough wave height (one height is extracted between zero downcrossing points for the wave elevation during the wave calibration tests). Similar to the observations of Hansen et al. [12], for the most severe sea states, the empirical deep water distribution from Forristall [22] tends to underestimate intermediate wave heights and overestimate the largest wave heights. For the sea state with H_s 6.8 m and T_p 13.2 s, the Forristall distribution agrees well with the experimental results.

3.2. Monopile responses

Fig. 4 also shows the exceedance probability distribution for selected monopile responses. For comparison with the work by Bredmose et al. [10], for each response, a single maximum value in between zero downcrossings of the wave elevation is chosen. The results in Fig. 4 highlight the importance of the steepness of the sea state: the extreme accelerations, shear forces, and base bending moment tend to be larger for the highest s rather than the largest H_s. Furthermore, increasing the damping ratio tends to decrease the accelerations and bending moment for the main body of responses ($P_{exc} > 0.01$), but does not have a significant effect on the largest events. The increase in damping was only tested for the smallest sea state. Further work is needed to determine whether the same conclusions hold for more severe sea states, and whether or not similar results can be reproduced numerically.

Although direct comparison to the WaveLoads experimental results [10] is difficult due to differences in the sea states, water depth, and structural characteristics, some differences in the shape of the distributions are worth noting. For the accelerations, most results in Fig. 4 show a fairly linear trend (on a logarithmic y axis) for $P_{exc} < 0.1$. Four of the seeds show some extrema that deviate from the linear trend. The acceleration results for the smallest sea state in the WaveLoads project for 30.8 water depth are more similar to the four seeds that are outliers in the present results. The WaveLoads results for the larger sea state are qualitatively more similar in shape to the majority of the present results, but if one considers the ratio between the maximum acceleration and the $P_{exc} = 0.01$ acceleration, the present results show a much smaller ratio; that is, the extreme accelerations in the present results are more similar to more frequently occurring accelerations.

For extreme events, the WaveLoads experimental results for base shear follow qualitatively similar trends as the acceleration in the same experiments [10]. In their results, the maximum base shear is roughly 3 times larger than the force corresponding to $P_{exc} = 0.01$. In contrast, the present work shows few relatively large individual extremes for base shear. The maximum base shear is typically 1.1 to 1.3

times larger than the force corresponding to $P_{exc} = 0.01$. Increasing the structural damping has little effect on the exceedance probability distribution for base shear.

The bending moment at the seabed was not measured in the WaveLoads results. Similar to the base shear, the results for the bending moment in Fig. 4 are fairly linear (on a logarithmic y axis). Unlike the base shear, the main body of bending moment responses for the two most severe sea states are quite similar.

The results in Fig. 4 also highlight the need for multiple realizations when examining the distribution of responses: there is a significant spread in the results even at $P_{exc} = 0.1$ (approximately 10 % for the bending moment, 16 % for the base shear, and 20 % for the acceleration in H_s 8.6 m, T_p 11 s), and the shape of the tail of the distribution can vary significantly among realizations.

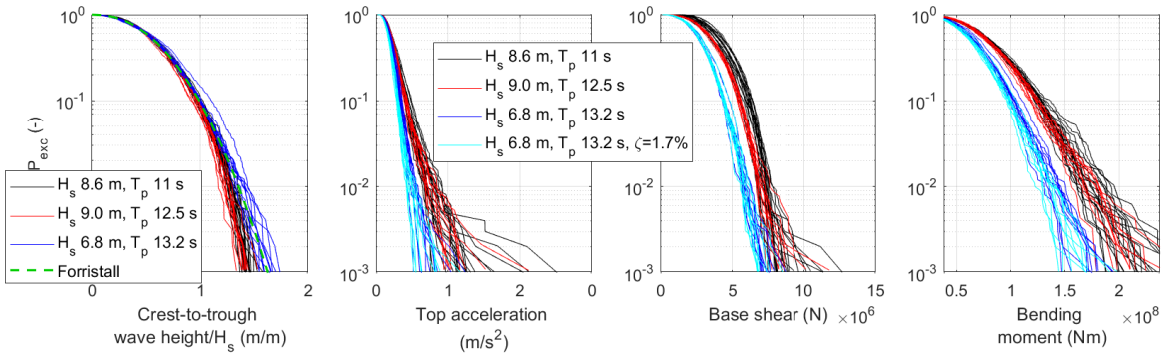

Figure 4: Exceedance probability distribution for the crest-to-trough wave height, horizontal acceleration at the top of the model, base shear force and base bending moment. One maximum per wave downcrossing.

3.2.1. Modal contributions to bending moment, shear force, and acceleration Following Suja-Thauvin et al. [2], we also filter the responses into contributions near the first and second natural frequency (denoted f_1 and f_2) and a remaining quasi-static component (QS). Figs. 5 and 6 show examples of the decomposition of the responses for two events. The events are selected based on the bending moment.

Suja-Thauvin et al. furthermore examine contributions at the exact time of the maximum total response for selected events in the WiFi data [2]. This decomposition is intended to illustrate the importance of resonant excitation of different modes. While such an approach gives useful insights, especially when comparing against numerical models, the approach is sensitive to the phase of the responses in different frequency bands. Furthermore, the first mode response often increases for several cycles after the maximum response. Therefore, we additionally consider the maxima in different frequency bands within $[-T_p, 2T_p]$ of the total maximum. In Figs. 5 and 6, for the bending moment, these two different approaches are shown by circles (simultaneous contributions) and x's (maximum contributions within $[-T_p, 2T_p]$).

Fig. 5 shows an event ("Event 1") with little contribution at the natural frequency of the second mode, while the bending moment and acceleration responses contain significant responses at the first natural frequency. Fig. 6 shows an event ("Event 2") with significant response at the natural frequency of the second mode. The component of the response characterized as quasi-static is particularly important for the base shear in both cases, while, as expected, there is negligible quasi-steady response for the accelerations. As in the WaveLoads experiments, the wave loads are inertia-dominated, and the base shear force is correlated with the time derivative of the wave elevation.

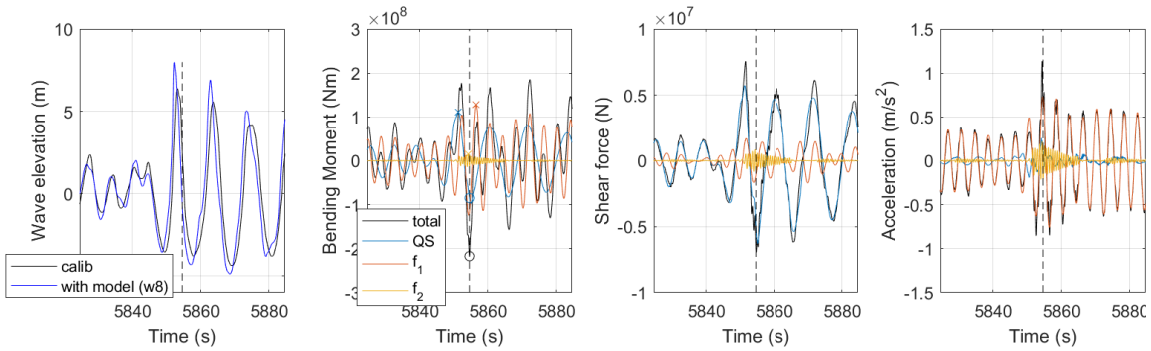

Figure 5: Decomposition of responses, event 1 (H_s 8.6 m, T_p 11 s). In the bending moment results, circles show the contributions at the instant of the maximum total response, while x's show the maximum result within $[-T_p, 2T_p]$ of the time of occurrence of the maximum total response.

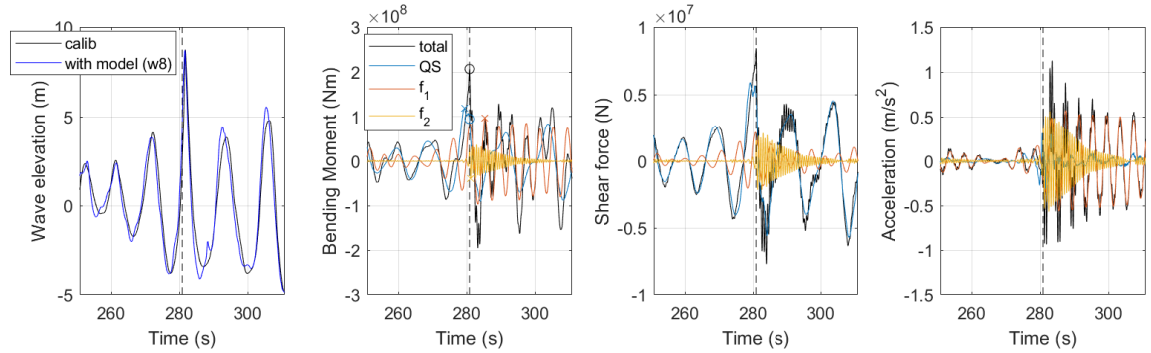

Figure 6: Decomposition of responses (as in Fig. 5), event 2 (H_s 8.6 m, T_p 11 s).

From each realization of each sea state, four independent (separated by at least $5T_p$ in time) bending moment maxima were identified. For each event, the relative contributions were assessed using the two methods previously described: Fig. 7 shows the contributions at the instant of the maximum total response, while Fig. 8 shows the relative magnitude of the response near the maximum total responses. In order for the total of the contributions to be 100 %, the second method divides the contributions by the sum of the individual contributions, but the abscissa still represents the actual maximum total response. The repetitions are not shown here, and some sea states have more realizations than others.

Figs. 7 and 8 show qualitatively similar results: the importance of the quasi-static response decreases for the largest events, while the importance of the responses at the second mode natural frequency tends to increase. There is no clear trend for the responses near the first natural frequency. The first method suggests a classification of the relative contributions such as QS: 40-70 %, f_1: 30-60 %, f_2: 0-25 %; using the second method would result in QS: 35-65 %, f_1: 30-60 %, f_2: 0-30 %. These results agree generally with the WiFi results [2], although the correlation between the second eigenfrequency and wave breaking has not yet been investigated in the present results.

3.3. Correlation between acceleration and wave breaking limits

To compare against WaveLoads data presented by Bredmose et al. [10], the peak acceleration identified in between two wave elevation downcrossings is shown in Fig. 9 as a function of a steepness parameter, H/L_0 and a depth parameter h/L_0. Here, H is the crest-to-trough wave height, h is the water depth, and L_0 is the deep water wavelength associated with the downcrossing period of the individual wave. The wave breaking lines are identical to those presented by Bredmose et al. [10] following Goda's work [23].

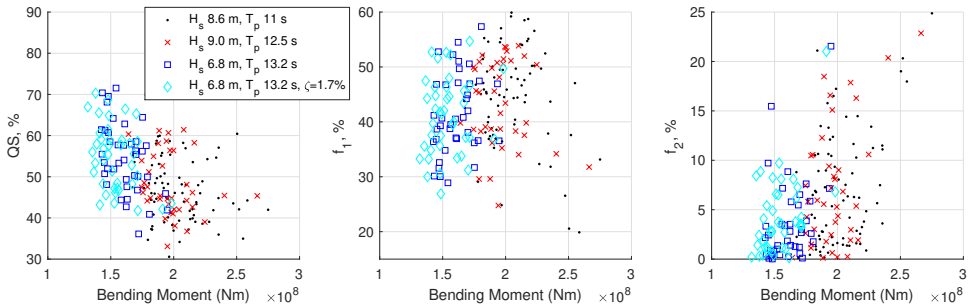

Figure 7: Relative contribution of different frequency bands to selected events. Contributions calculated at the instant of the maximum total response. Repetitions are not included.

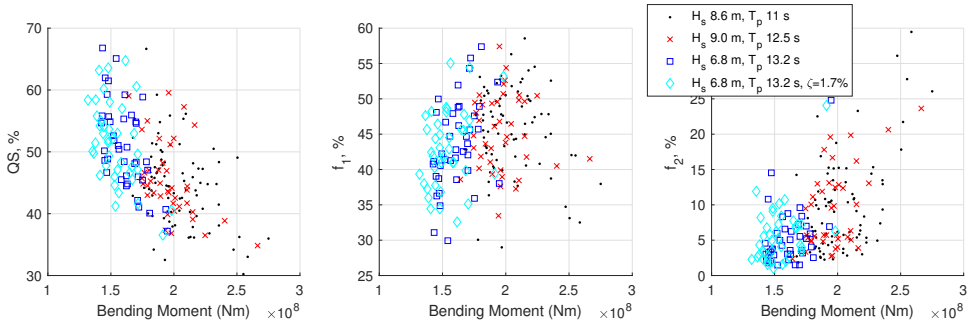

Figure 8: Relative contribution of different frequency bands to selected events. Contributions calculated by the maximum value in that frequency band within $[-T_p, 2T_p]$ of the time of maximum total response. The contributions are divided by sum of the three contribution obtained in this manner (such that the total relative contribution is 100 %), but are plotted as a function of the total maximum.

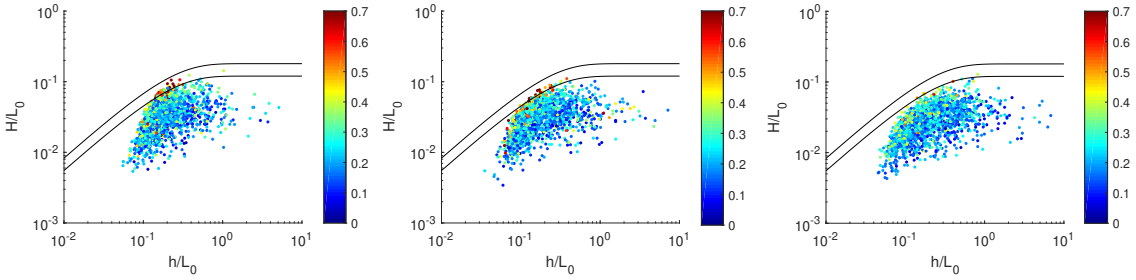

(a) H_s 8.6 m, T_p 11 s **(b)** H_s 9.0 m, T_p 12.5 s **(c)** H_s 6.8 m, T_p 12.3 s

Figure 9: Acceleration at the nacelle (color scale in m/s^2) plotted based on a steepness parameter and depth parameter for individual wave events. Two realizations (seeds) for each sea state are included.

Similar to the WaveLoads data, large accelerations near the wave breaking limit can be observed. On the other hand, compared to the WaveLoads data, a larger number of high accelerations can also be observed far from the wave breaking limit, and for larger values of the depth parameter.

3.3.1. Repeatability The extensive repetitions of selected seeds allow a brief investigation of the random uncertainty in the experimental results. Fig. 10 shows all 15 repetitions of events 1 and 2 from Figs. 5 and 6, while Fig. 11 shows the coefficient of variation (COV, standard deviation divided by the mean) for the 10 largest events in one seed with H_s 8.6 m and T_p 11 s.

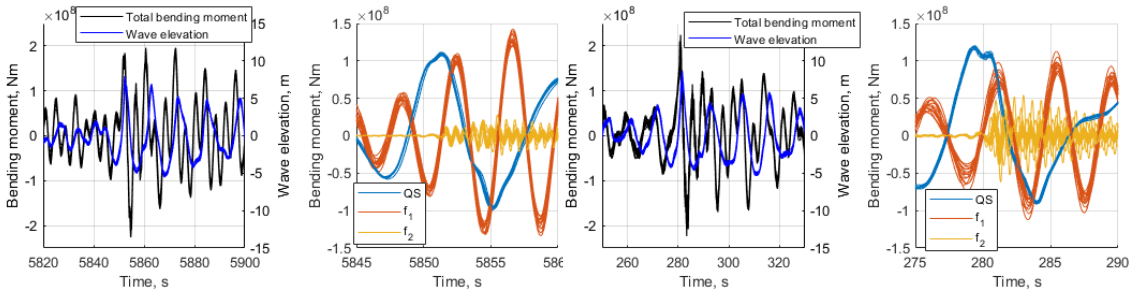

(a) Event 1 **(b)** Event 2

Figure 10: Repeatability of wave and bending moment, including decomposition of bending moment for all repetitions. 15 repetitions are shown. The wave elevation shown here is from gauge 8 (Fig. 2) during the tests with model.

The time series results show that the quasi-static responses have a very high degree of repeatability, while the responses at higher frequencies show larger spread. The responses near the natural frequency of the second mode, especially for event 2, are quite variable. For the two events that are shown, the phasing of the first mode response is in good agreement. Compared to the results from the NOWITECH tests [11], the increased damping in the present tests may explain the improved repeatability of the phase of the responses at the first natural frequency. The present results may therefore prove more useful for validation of numerical tools.

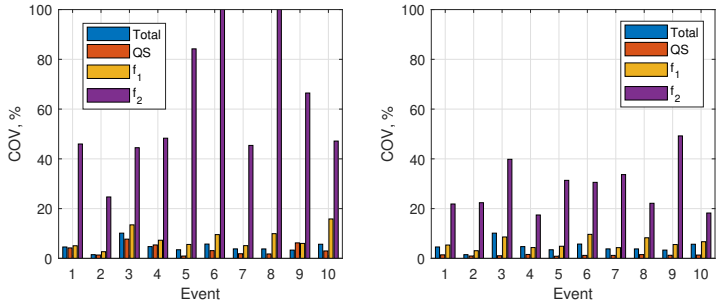

Figure 11: Coefficient of variation (COV) for the 10 largest bending moment maxima in 15 repetitions of one seed with H_s 8.6 m and T_p 11 s. Left: contributions calculated at the exact time of the maximum total moment. The largest COV exceeds 200 %. Right: maximum of each contribution within $[-T_p, +2T_p]$ of the maximum total moment.

The COV in Fig. 11 confirms that similar results can be seen across other events: the quasi-static responses have COV of less than 8 % for Suja-Thauvin's definition of the contributions, and less than 2 % for the alternative definition. The COV for the total bending moment (identical in both left and right side of Fig. 11) and for the contribution near the first natural frequency is less than approximately 10 %, while the corresponding results for the responses near the second natural frequency are to almost 50 %, even for the definition of the contributions which is less sensitive to phasing differences. The lower COV for the total bending moment compared to the NOWITECH tests is likely due to the increased structural damping.

4. Conclusions

The main characteristics and selected results from an experimental campaign with a flexible, 9 m diameter monopile wind turbine in severe waves are documented in the present work. These results

are compared against published results with similar flexible structures. Compared to the previous campaigns, the larger diameter, inclusion of several damping levels, and increased number of realizations and repetitions allow for drawing new conclusions.

Compared to previous results, some qualitative differences in the exceedance probability distribution of the nacelle acceleration and base shear were noted. Contributions from responses at the first and second natural frequencies, and at lower frequencies, were similar to previous results, although a clearer trend in increasing response at high frequencies for the largest events was documented here. The relative contributions were not very sensitive to minor adjustments in how these contributions were evaluated, while the repeatability was. The correlation between large nacelle accelerations and the wave breaking limits was not as clear as in previous tests.

While the present work provides some interesting comparisons among different results, further analysis is needed in order to explain the reasons for the differences. Numerical simulations, more detailed study of the videos of various events, investigation of the effects of second order corrections in the wavemaker signal, and further statistical analysis of the results are planned in future work. Increased accuracy of numerical tools through validation can lead to improved design solutions.

Acknowledgments

The authors gratefully acknowledge the support from the Wave Loads and Soil Support for Extra Large Monopiles (WAS-XL) project (NFR grant 268182). Parallel analysis by Elise Moen is also appreciated.

References

[1] Faltinsen O M, Newman J N and Vinje T 1995 *Journal of Fluid Mechanics* **289** 179–198
[2] Suja-Thauvin L, Krokstad J R, Bachynski E E and de Ridder E J 2017 *Ocean Engineering* **146** 339–351
[3] Kristiansen T and Faltinsen O M 2017 *Journal of Fluid Mechanics* **833** 773–805
[4] Stansberg C T 1997 *8th International Conference on the Behaviour of Off-Shore Structures (BOSS'97)* vol 2 pp 95–112
[5] Bachynski E E, Kristiansen T, and Thys M 2017 *Applied Ocean Research* **68** 154–170
[6] Riise B H, Grue J, Jensen A and Johannessen T B 2018 *Journal of Fluid Mechanics* **853** 564–586
[7] de Ridder E J, Aalberts P, van den Berg J, Buchner B and Peeringa J 2011 *ASME 2011 30th International Conference on Ocean, Offshore and Arctic Engineering* OMAE2011-49563
[8] de Ridder E J, Bunnik T, Peeringa J M, Paulsen B T, Wehmeyer C, Gujer P and Asp E 2017 *ASME 2017 36th International Conference on Ocean, Offshore and Arctic Engineering.* OMAE2017-62040
[9] Nielsen A W, Schlütter F, Sørensen J V T and Bredmose H 2013 *ASME 2012 31st International Conference on Ocean, Offshore and Arctic Engineering* OMAE2012-83533
[10] Bredmose H, Slabiak P, Sahlberg-Nielsen L and Schlütter F 2013 *ASME 2013 32nd International Conference on Ocean, Offshore and Arctic Engineering* OMAE2013-10948
[11] Bachynski E E, Thys M and Delhaye V 2019 *Applied Ocean Research* **89** 96–114
[12] Hansen H F, Lohmann I P, Sørensen J T and Schlütter F 2012 *ASME 2012 31st International Conference on Ocean, Offshore and Arctic Engineering* OMAE2012-84114
[13] Li L, Gao Z and Moan T 2013 *ASME 32nd International Conference on Ocean, Offshore, and Arctic Engineering* OMAE2013-10156
[14] Velarde J and Bachynski E E 2017 *Energy Procedia* **137** 3 – 13 ISSN 1876-6102 14th Deep Sea Offshore Wind R&D Conference, EERA DeepWind'2017
[15] Damgaard M, Andersen J K, Ibsen L B and Andersen L V 2012 *Proceedings of the Twenty-second (2012) International Offshore and Polar Engineering Conference* pp 300–307
[16] Damgaard M, Ibsen L, Andersen L and Andersen J 2013 *Journal of Wind Engineering and Industrial Aerodynamics* **116** 94 – 108 ISSN 0167-6105
[17] Shirzadeh R, Weijtjens W, Guillaume P and Devriendt C 2014 *Wind Energy* **18** 1685–1702
[18] Devriendt C, Jordaens P J, Sitter G D and Guillaume P 2013 *IET Renewable Power Generation* **7** 401–412 ISSN 1752-1424
[19] Devriendt C, Weijtjens W, El-Kafafy M and Sitter G D 2014 *IET Renewable Power Generation* **8** 433–441 ISSN 1752-1424
[20] Schäffer H A 1996 *Ocean Engineering* **23** 47–88
[21] Bachynski E E, Kristiansen T and Thys M 2017 *Applied Ocean Research* **68** 154–170
[22] Forristall G Z 1978 *Journal of Geophysical Research: Oceans* **83** 2353–2358
[23] Goda Y 2010 *Coastal Engineering Journal* **52** 71–106